



Biologically Inspired Girder Structure for the Synchrotron Radiation Facility PETRA IV

Simone Andresen¹ · Norbert Meyners² · Daniel Thoden² · Markus Körfer² · Christian Hamm¹

Received: 10 October 2022 / Revised: 16 March 2023 / Accepted: 21 March 2023
© The Author(s) 2023

Abstract

Lightweight structures are widely used across different industry sectors. However, they get easily excited by external influences, such as vibrations. Undesired high vibration amplitudes can be avoided by shifting the structural eigenfrequencies, which can be achieved adapting the structural design considering optimisation procedures and structures primarily inspired by diatoms. This procedure has been applied to the development process of a girder structure installed in a synchrotron radiation facility to support heavy magnets and other components. The objective was to design a 2.9 m long girder structure with high eigenfrequencies, a high stiffness and a low mass. Based on a topology optimisation result, a parametric beam-shell model including biologically inspired structures (e.g., Voronoi combs, ribs, and soft and organic-looking transitions) was built up. The subsequent cross-sectional optimisation using evolutionary strategic optimisation revealed an optimum girder structure, which was successfully manufactured using the casting technology. Eigenfrequency measurements validated the numerical models. Future changes in the specifications can be implemented in the bio-inspired development process to obtain adapted girder structures.

Keywords Biomimetics · Eigenfrequency maximisation · Evolutionary structural optimisation · Lightweight design · Topology optimisation · Voronoi combs

1 Introduction

Lightweight structures are widely used across different industry sectors, e.g., in the field of mobility or robotics. However, in contrast to heavy, massive constructions,

lightweight structures get easily excited by external influences, such as vibrations [1]. Thus, finding the optimum structural design to avoid high vibration amplitudes has become very important, especially with recent demands for high performance lightweight structures. In addition, the global goal to reduce emission motivates the development of improved lightweight structures. To reduce high vibration amplitudes, the structural mass is traditionally increased and/or damping devices are implemented [2]. However, the resulting mass increase is contrary to the original goal of lightweight structures. In addition, active damping systems are weak points of the system and ‘react time-delayed’.

A vibrating system is defined by the mass, the elastic properties and the damping properties. Another approach to avoid high vibration amplitudes is to adapt the structural design. As a consequence, the elastic properties (i.e., stiffness) and/or the mass are changed, as well as the structure’s eigenfrequencies. Thus, resonance phenomena, which occur when the external frequency matches an eigenfrequency of the system and often lead to high vibration amplitudes, can be prevented. This approach to raise (maximise) eigenfrequencies shows a high potential to be applied to lightweight

✉ Simone Andresen
simone.andresen@awi.de

Norbert Meyners
norbert.meyners@desy.de

Daniel Thoden
daniel.thoden@desy.de

Markus Körfer
markus.koerfer@desy.de

Christian Hamm
christian.hamm@awi.de

¹ Bionic Lightweight Design & Functional Morphology, Alfred Wegener Institute Helmholtz Centre for Polar and Marine Research (AWI), Am Handelshafen 12, 27570 Bremerhaven, Germany

² Deutsches Elektronen-Synchrotron (DESY), Notkestraße 85, 22607 Hamburg, Germany

structures, because it does not necessarily imply a mass increase.

Many published studies deal with structural optimisations to find an optimum material distribution with the objective to maximise eigenfrequencies. Most focus has been put on topology optimisations. A topology optimisation problem involves the determination of the physical size and the shape and connectivity of a structure, while the boundary conditions, the design space, and the targeted volume are predetermined [3]. Topology optimisations to increase the 1st structural eigenfrequency were first considered by [4]. Since then, numerous studies on topology optimisations to increase eigenfrequencies have been published, e.g., [5–8], showing the relevance of this topic. Eigenfrequencies were also maximised using evolutionary structural optimisation [9, 10] or bidirectional evolutionary structural optimisation [11, 12]. However, most of the mentioned studies focused on 1D and 2D structures. Topology optimisations have also been combined with lattice structures (also called ‘lattice structure topology optimisation’) to improve mechanical properties, e.g., [13–15]. The later studied irregular, porous infills for additive manufactured structures inspired by cancellous bones. They showed that the biologically inspired infills were 1.5 times stiffer than honeycomb structures and 1.1 times stiffer than optimised rhombic structures.

Aside from the high relevance of the vibration issue in industry, also in nature, organisms have to deal with undesired structural vibrations. While most technical lightweight structures, e.g., honeycomb sandwich constructions, lattice structures or truss structures, have mainly regular geometries, natural lightweight structures are often complex and show good mechanical properties, such as honeycombs of bees [16], the beak of toucans [17, 18], cancellous bones [16, 19], or the shell structures of diatoms [20]. These structures are highly optimised during the process of evolution and usually fulfil different functions. In particular, diatoms with biomineralised cell covers have developed a high diversity of irregular structures. As these plankton organisms need to float in the nutritious upper water column to survive and also carry out photosynthesis, their silicate shells must be very light. At the same time, high structural stiffness and stability is essential to stand the attacks by their predators, the copepods. Thus, the combination of low mass and high stiffness leads to lightweight design principles that can be observed in these biological structures [21–24]. Although these complex structures follow the same basic construction principles of technical structures using ribs, lattices, and honeycombs [24], they are highly multifunctional characterised by a high permeability [25], mechanical robustness [26], high energy absorption [22], and vibration optimisation [27]. In regard to the good mechanical properties of diatom shells, their lightweight design principles serve already as inspiration for

lightweight construction and have been successfully applied to structures across different industrial sectors [28–30].

Besides the lightweight design principles observed in diatom shell structures, a high impact of these irregular structures on the vibration characteristics is expected, since the copepod’s attacks do not only involve high point loads, but the predators also hammer on their prey with Reynold’s numbers of 10^{-2} to 10^{-1} , or rather, the feeding tools move at rates of 20–80 Hz [31]. Consequently, the cell cover has to be resilient against vibrational load cases. However, *in vivo* experiments to measure the diatom shell eigenfrequencies have not been possible up to now. Thus, construction and simulation of diatom shells are necessary to obtain more information about their vibration characteristics. In first studies, numerical modal analyses of abstracted diatom shells were performed [27]. They indicated that diatom shell mode shapes correlate well with deformation patterns that can be observed in these shells. Aside from this, little is known about the purpose of diatom cell covers as a result of challenges related to acoustic properties. However, it is obvious that the concept to generate, optimise, and apply such highly complex irregular structures allows the substantial manipulation of vibration properties [32].

In regard to technical honeycomb and lattice structures, most research has investigated the static mechanical properties, while little is known about their dynamic properties, in particular, their vibration properties. Several studies have been conducted on sandwich beams or plates with lattice or honeycomb core designs (beams: [33–37], plates: [14, 38–40]). Very few investigations dealt with the vibration properties of larger scaled lattice structures [41, 42]. However, in all mentioned studies, the structural design was regular. In regard to irregular structures, the 1st eigenfrequency of honeycomb plates has been increased using irregular Voronoi cell structures inspired by diatom shells [43]. The 1st eigenfrequency of 3D structures composed of cubic lattices was also risen owing to the application of irregular cross section diameters to the lattice struts [44]. In other lattice structures, irregular cross-sectional diameters also lead to a significant 1st eigenfrequency increase [45]. In the later study, the 1st eigenfrequency was shifted to even higher values using an irregular lattice strut designs.

To sum up, the vibration properties of structures are often improved conducting common structural optimisations. However, recently, first studies indicated a high impact of irregular honeycomb and lattice structures on the vibration properties. In the present work, common optimisation procedures are extended using optimisation procedures and irregular structures inspired primarily by diatoms. It is focused on a magnet girder structure installed in a synchrotron radiation facility, for which high eigenfrequencies, a high stiffness and a low mass are demanded.

Synchrotron radiation facilities are powerful machines that allow detail investigations of structures, materials, and processes at different time and length scales *in situ* *in vivo* [46]. The heart of a synchrotron radiation facility is a storage ring, in which electrons circle at a constant energy. Synchrotron radiation is generated by deflecting the electrons' trajectory with the help of magnetic fields [47]. The numerous magnets are placed on girders along the particle beam path.

All synchrotron radiation sources worldwide are limited in spectral brightness [46]. However, very parallel and narrow particle beams generate high-intensity X-rays, which allow an even more detailed investigation of samples in the microscopes. Thus, a new (fourth) generation of synchrotron sources has been developed based on stronger focussing magnets to generate even smaller and more intense X-rays. At DESY (Deutsches Elektronen-Synchrotron, Hamburg, Germany), the synchrotron radiation facility PETRA IV (Positron-Elektron-Tandem-Ring-Anlage; en: Positron Electron Tandem Ring Facility) is currently planned [46, 48]. The new PETRA IV light source will be very sensitive towards external vibrations, which is why the magnet-girder assemblies along the particle beam have to be re-designed.

The stability of particle beams depends, aside from the thermal issues, on the transfer function of the ground vibration to the particle beam [49]. Regarding the first, the temperature inside the PETRA tunnel will be stabilised to ± 1 K [48] to avoid strong movements or deformations of tunnel segments or machine components, such as girders. As for the vibration issue, the girder plays a major role in the vibration transmission path from the ground vibrations to the particle beam [50].

Soft magnet-girder assemblies would allow an vibration isolation from the ground motion. However, they cannot be installed in the PETRA IV machine, as they would not meet the low tolerances between neighbouring girders. Thus, a high stiffness of the magnet-girder assemblies is essential to meet the girder positioning tolerance and to reach high structural eigenfrequencies. The later permits a low vibration transmissibility [50, 51].

The main requirements for the biologically inspired girder to be designed are:

1. High eigenfrequencies: All eigenfrequencies shall be above 30 Hz [51], because ground vibrations at DESY strongly drop with increasing frequency [52]. As the numerically obtained eigenfrequencies are often higher than the actual ones, the objective is to reach a 1st eigenfrequency of about 50 Hz in the numerical models.
2. A high stiffness: Because of heavy components mounted to the girder, a high stiffness is essential for low static deflections due to gravity. In addition, a high stiffness usually leads to high eigenfrequencies.

3. Low structural mass: The girder shall be light to keep the total weight of a fully equipped girder assembly as low as possible to allow a transportation of the girder equipped with the already heavy magnets.

An overview on magnet-girder assemblies of different accelerators worldwide has been published [49]. The 1st eigenfrequencies of the magnet-girder assemblies vary from about 10 Hz of the 3rd generation machines (European Synchrotron Radiation Facility [ESRF], Advanced Photon Source [APS]) to above 40 Hz for the new-generation light sources (French national synchrotron facility SOLEIL, ESRF-Extremely Brilliant Source [ESRF-EBS]). The 1st eigenfrequency of the currently operating PETRA III girder is about 35 Hz and of the 1st magnet mode about 25 Hz [53]. A model of the PETRA III girder installed in the 2.3 km long PETRA tunnel is displayed in Fig. 1. The tunnel will also be used for the upgraded machine, which is why the dimensions of the girder designed here followed the PETRA III girder geometry.

So far, most girders have box-like structures. However, new design approaches have been made, e.g., at the Argonne National Laboratory, where topology optimisations of the APS Upgrade (APS-U) girder combined with thickness optimisations of the upper solid girder plate allowed a 1st eigenfrequency increase towards 39 Hz for a 6.5 m long ductile cast iron (GR-60/40/18) girder considering three support points [54, 55].

To sum up, in this study, a biologically inspired development process is presented. The objective is to design a girder structure installed in a synchrotron radiation facility which shows high eigenfrequencies, a high stiffness and a low mass. The applied optimisation techniques and structural elements are primarily inspired by diatoms.

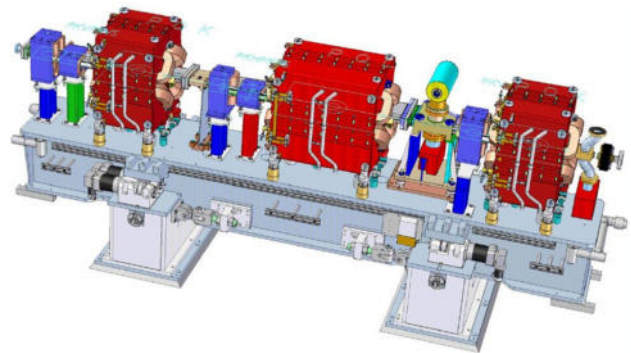


Fig. 1 Model of a 4.2 m long PETRA III girder that is positioned on two bases and equipped with several components including three large magnets (red). The figure is printed according to [48] with permission from Deutsches Elektronen-Synchrotron DESY

2 Materials and Methods

The development of a biologically inspired girder design for PETRA IV involved different steps, which are summarised in Fig. 2. After the definition of the specifications, a topology optimisation was performed to disclose an optimum material distribution. However, a topology optimisation only indicates, where material should be placed or removed and does not present an optimum dimensioned structure. Figure 3 shows exemplary the development process of an optimised 2D structure with the objective to increase the stiffness at reduced mass. Based on the defined boundary conditions and load cases, the topology optimisation identifies an optimum material distribution. The abstraction of the topology optimisation result allows the creation of a beam model with an initial constant cross-sectional diameter. Subsequently, a cross-sectional optimisation shows the optimum dimension of each strut. The result clearly varies from the cross-sectional dimensions obtained by the topology optimisation. Finally, the structure was partly adapted, e.g., replacing sharp corners by smooth connections and thickening critical intersection points to allow a successful manufacturing process.

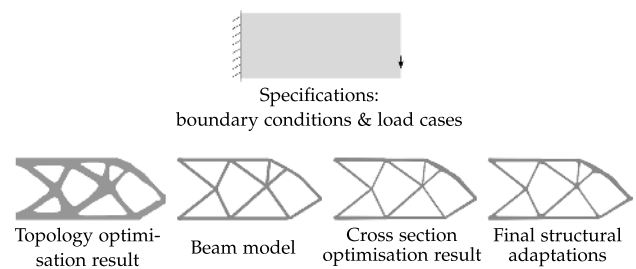
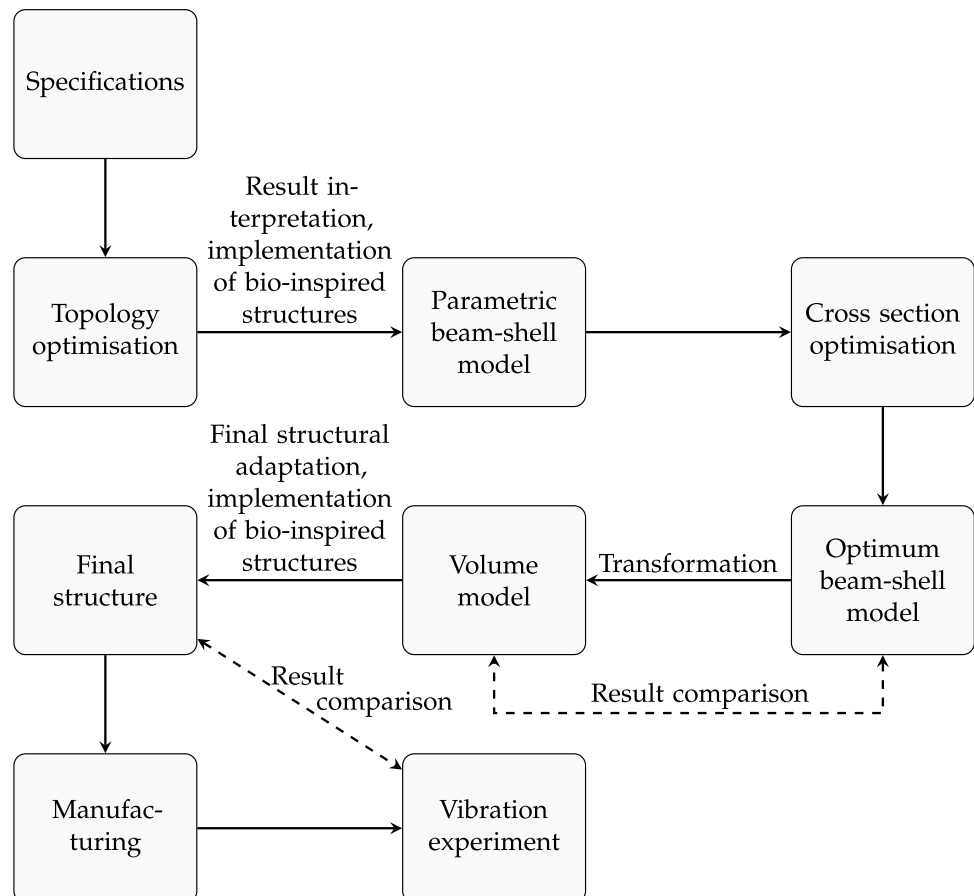


Fig. 3 Development of an optimised 2D structure based on the given specifications. The process comprised a topology optimisation, the development of a beam model, a cross-sectional optimisation, and the finalisation of the structure implementing small structural adaptations, e.g., rounding of sharp edges and corners

Thus, also here, the topology optimisation served as an inspiration for an optimum material distribution within the defined design space. The topology optimisation result was interpreted and abstracted, before, in combination with the implementation of biologically inspired structures, a parametric beam–shell model of the girder was created. The subsequent cross-sectional optimisation using the evolutionary strategy led to numerous structures that were evaluated. After transforming the best structure into a volume model,

Fig. 2 Overview of the girder design procedure including nine steps



the results of both the beam–shell and the volume model were compared to identify a possible deviation of the results using a comparably fast calculating beam–shell model. The volume model was then improved implementing further biologically inspired structures. Last structural adaptations demanded by changes in the specifications and by special requirements regarding the manufacturing process led to the final girder structure. After the manufacturing process, the eigenfrequencies and mode shapes were measured performing impact tests and compared to the numerical results obtained for the volume model.

The girder design process was build using the software Rhinoceros (version 6 SR10, Robert McNeel & Associates, Seattle, WA, USA) with its Plug-In Grasshopper (version 1.0.0007, Robert McNeel & Associates). The numerical solver was OptiStruct (Altair Engineering Inc., Troy, MI, USA).

2.1 Specifications

Prior to the design process of the biologically inspired PETRA IV girder, a large parametric study investigated the impact of different boundary conditions and components on

the eigenfrequencies of the magnet–girder assembly [50]. The defined finite element model layout was also used here. It was based on a large girder design space of $2.90 \times 0.65 \times 0.80$ m, which was equipped with eight magnets and connected at three points to solid pedestals (bases) using beam elements (element type CBEAM) as displayed in Fig. 4. The beam elements had a solid circular cross section with a diameter of 50 mm. Steel S235 (Table 1) was assigned as material to the girder design space, the bases and the connecting beams. To simulate the real magnet masses, a specific artificial material density was defined for each magnet as listed in Table 2. For more information about this model layout it is referred to [50].

Table 1 Material properties of structural steel S235, grey cast iron (EN-GJL-350), and spheroidal cast iron (EN-GJS-700-2) considered within the present study involving the Young’s modulus E , the material density ρ , and the Poisson’s ratio ν

	S235	Grey cast iron	Spheroidal cast iron
E (N · mm ⁻²)	210,000	130,000	176,000
ρ (kg · m ⁻³)	7,800	7,300	7,200
ν (-)	0.30	0.26	0.28

Fig. 4 Top view (a), side view (b), and 3D view (c) of the general model assembly including the girder design space (grey), the three bases (green), the eight magnets (blue), and the three beams connecting the girder to the bases (red). The location of the particle beam is shown in magenta. All given dimensions are in mm. The figure is printed according to [50]

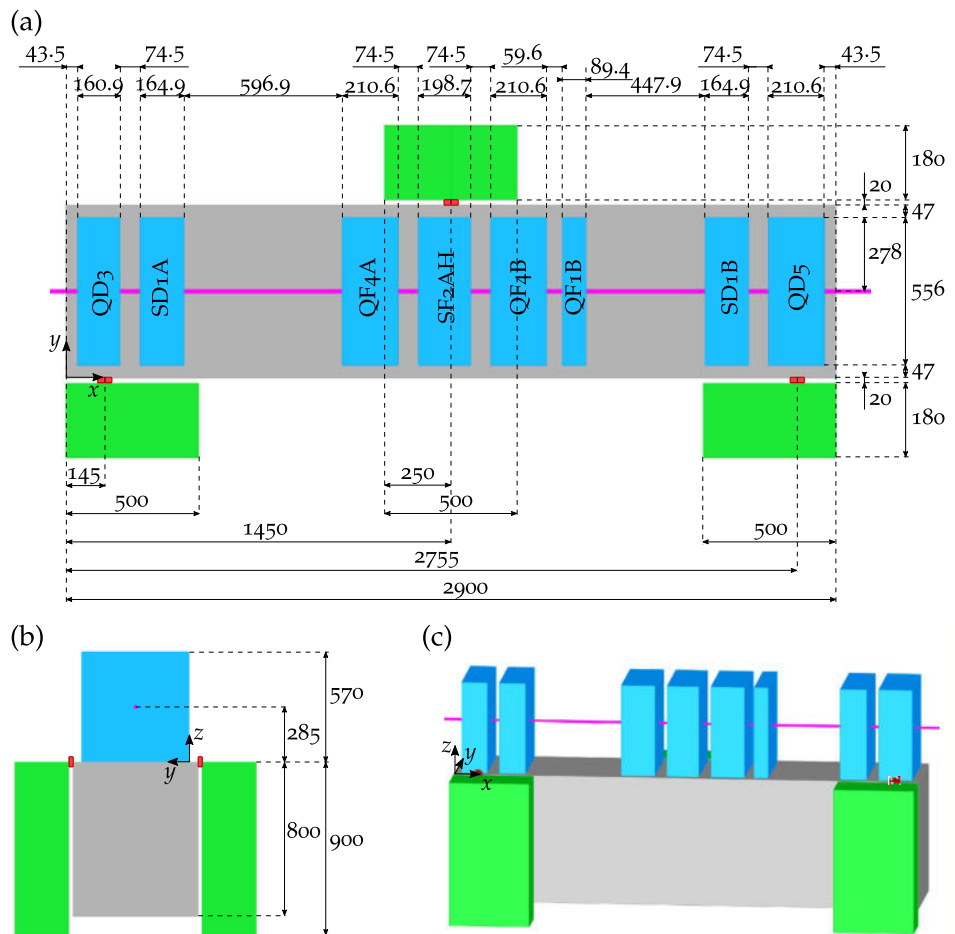


Table 2 Artificial material densities assigned to the magnets

Magnet	Material density
QD3	$3.496 \cdot 10^3 \text{ kg} \cdot \text{m}^3$
SD1A	$1.188 \cdot 10^4 \text{ kg} \cdot \text{m}^3$
QF4A	$4.825 \cdot 10^3 \text{ kg} \cdot \text{m}^3$
SF2AH	$1.187 \cdot 10^4 \text{ kg} \cdot \text{m}^3$
QF4B	$4.825 \cdot 10^3 \text{ kg} \cdot \text{m}^3$
QF1B	$1.563 \cdot 10^4 \text{ kg} \cdot \text{m}^3$
SD1B	$1.188 \cdot 10^4 \text{ kg} \cdot \text{m}^3$
QD5	$6.634 \cdot 10^3 \text{ kg} \cdot \text{m}^3$

Table 3 Number of volume mesh nodes and elements of the topology optimisation for the 3 m PETRA IV girder

	Number of nodes	Number of elements
Girder design space	279,541	1,574,726
Girder non-design space	17,150	50,181
Magnets	7,066	25,725
Bases	2,609	9,132
<i>Total</i>	306,366	1,659,764

2.2 Topology Optimisation

A topology optimisation was conducted to reveal an optimal material distribution. The model was built up following the mentioned specifications and the model assembly shown in Fig. 4. Thus, the design space, from which material was removed during the optimisation, was shaped like a box. However, the upper surface with a thickness of 20 mm was defined as non-design space, because a continuous upper girder surface was required for the later fixation of different components in the tunnel. The box girder was equipped with magnets and connected via beams to the bases. Consequently, the non-design space comprised, aside from the upper girder surface, the magnets, the bases, the connection beams, and the rigid body elements (element type RBE3) defined between the connection beams and both the girder and the bases.

The box girder, the magnets, and the bases were meshed with constant element sizes of 20 mm, 50 mm, and 100 mm, respectively, leading to a very fine mesh of the design space to allow the development of clear load paths during the optimisation. Table 3 lists the total number of nodes and elements.

All nodes of the lower bases' surfaces were considered as fixed (all translations = all rotations = 0). A modal load case to calculate the 1st eigenfrequency and a linear static load case to obtain the maximum static deformation due to gravity ($g = 9.81 \text{ m} \cdot \text{s}^{-2}$ in $-z$ direction) were defined.

The optimisation objective was to maximise the 1st eigenfrequency considering two constraints: a maximum volume fraction of 20% for material removal from the solid design space and a maximum static deformation due to gravity of 0.05 mm.

The topology optimisation result assigns to each element of the design space an artificial element density value. While a value of 1 indicates that the corresponding element is essential to reach the defined objectives, elements with low artificial density values are removed. Here, the threshold value of the artificial element density was chosen as low as possible to obtain a connected structure.

2.3 Abstraction and Cross-sectional Optimisation

The structure obtained from the topology optimisation was abstracted into a beam–shell model. For this, strut- and beam-like parts were replaced by lines (beams) and surface-like parts by surfaces (shells). Thick, surface-like parts were abstracted as surfaces stiffened by additional rectangular ribs or as sandwich structures with an inner core based on ribs oriented in 45° angles with respect to the horizontal.

All lines were divided into sections of about 50 mm length and considered as beam elements (CBEAM) that were connected to the upper solid plate via RBE3. The surfaces were meshed with an element size of 30 mm using triangle elements (CTRIA) and connected to the corresponding beams by sharing nodes. The top surface that had been defined as non-design space, the magnets, and the bases were considered as solids. In addition, the beams connecting the girder and the bases were included in the model.

Subsequently, an evolutionary strategic optimisation of the shell thicknesses and the beam cross-sectional diameters was performed using the optimiser Octopus implemented in used software Grasshopper that permitted a multi-objective optimisation considering various parameters. The optimisation objectives were (1) the maximisation of the 1st eigenfrequency, (2) the minimisation of the maximum deformation due to gravity, and (3) the minimisation of the girder mass. The 21 parameters involved 11 shell thicknesses (definition range for each thickness: 5.0–30.0 mm) and 10 beam cross-sectional diameters each varying in the range 20.0–70.0 mm. The population size was set to 100 and the stopping criterion was a maximum number of 20 generations. The Octopus settings that were taken into account are listed in Table 4 and are based on the default and recommended settings. The elitism was set to 50%, as this value in combination with a mutation rate of also 50% is expected to lead to a successful optimisation [56].

All structures forming the last generation were considered for evaluation choosing the structure with the highest 1st eigenfrequency as the girder structure with an optimum parameter combination. With the help of different

Table 4 Octopus settings involving the hypervolume estimation algorithm (HypE)

Algorithm setting	Value
Elitism	0.5
Mutation probability	0.1
Mutation rate	0.5
Cross over rate	0.8
Population size	80
Maximum generations	20 (stopping criterion)
HypE reduction	Yes
HypE mutation	Yes

algorithms implemented in the Grasshopper-based module ELISE (Synera GmbH, www.synera.io), the beam-shell model was transferred into a volume model that was also evaluated regarding its eigenfrequencies, mode shapes, and maximum static displacement due to gravity ($g = 9.81 \text{ m}\cdot\text{s}^{-2}$ in $-z$ direction). A comparison of the results obtained by the volume model to those based on the beam-shell model indicated whether the fast calculating beam-shell model had already revealed plausible results.

2.4 Biologically Inspired Structures and Further Structural Adaptation

Based on the numerical results of the previous section, structural adaptations of the girder were performed. The 1st mode shape of the optimised girder structure showed a bending of the large lower strut. To avoid this deformation and to raise the corresponding eigenfrequency, a vertical strut was implemented in the middle front of the structure connecting the large lower strut to the upper girder surface.

Subsequently, the structure was provided with different biologically inspired structural elements to further improve both the mechanical properties and the design. Table 5 presents and describes all biologically inspired structures implemented in the girder design.

Due to posterior changes in the specifications by DESY, further structural changes have been applied to the designed girder. These changes involved a small reduction of the girder design space, which led to the removal of a small amount of material at the left girder side close to the base. In addition, the girder structure was slightly adapted to create space for a middle, inner screw. In the areas of the support point positions, material was added horizontally to fix the girder on machine shoes that allow a later vertical adjustment and connect the girder to the bases. At DESY, it was decided to use the machine shoe type UMS5-KDSA (isoloc Schwingungstechnik GmbH, www.isoloc.de).

In the final vibration experiments, the eigenfrequencies and the mode shapes of the unloaded girder positioned on soft springs were measured. To compare the numerical results to those obtained by the experiments, the eigenfrequencies and the mode shapes of the free and unloaded bio-inspired girder were calculated specifying grey cast iron (EN-GJL-350) as girder material (cf., material properties in Table 1). In addition, the 1st eigenfrequency of the free and unloaded PETRA III girder of 4.2 m length currently installed in the tunnel (Fig. 1) was also calculated considering grey cast iron as girder material and compared to that of the bio-inspired girder.

After that, the magnets, the bases provided by DESY, and the machine shoes were included into the model to obtain the eigenfrequencies, the mode shapes, and the maximum deformation due to gravity of the magnet-girder assembly. For the bases, spheroidal cast iron (EN-GJS-700-2) was defined as material (cf., material properties in Table 1). The machine shoes were abstracted as solid cylinders made of steel S235 following the dimensions of the already mentioned machine shoe type UMS5-KDSA. For all model components, a fine volume mesh was used as characterised in Table 6.

2.5 Manufacturing and Impact Testing

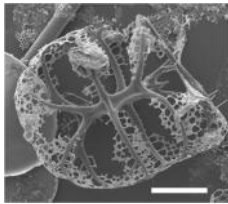
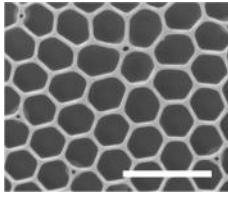
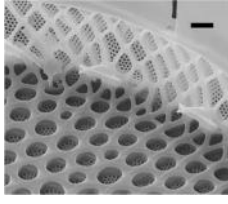
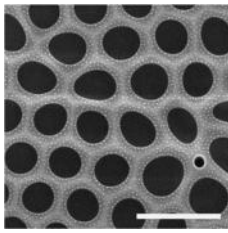
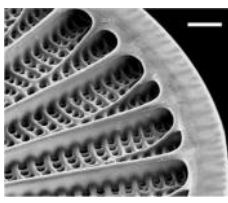
The designed girder structure was manufactured by the foundry Wurzen GmbH (Wurzen, Germany) using the casting technology in connection with 3D printed sand moulds. Grey cast iron (EN-GJL-250) was used due to its low ductility [57], which supported the filling of the complex mould. Wurzen GmbH also took care of additional adaptations of the manufactured part requested by DESY, including bore holes, notches, and a high surface evenness.

Impact testing was conducted at DESY to measure the eigenfrequencies of the free and unloaded girder, and thus to verify the simulations. The girder was positioned on three springs to abstract the free positioning (cf., Fig. 15). Eight uniaxial accelerometers (Type 4507 B 005, Brüel & Kjær) were fixed with bee wax to the upper girder surface at the different positions shown in Fig. 5. Using a recoilless hammer (Halder Supercraft 3377.050, 1.15 kg), the girder was hit through a rubber mat at the positions 4 and 8. Subsequently, the accelerometers were fixed to one pedestal and to the floor next to the set up to measure the vibrations of the pedestal and the floor. After converting the analog signals into digital signals using the ADC Data Translator DT9857E-08, the custom-made software VSI DataServer (Mark Lomperski, DESY) was utilised to store the data and perform the Fourier transformation to obtain the Power Spectral Density (PSD) of the girder.

The measured first five eigenfrequencies of the girder corresponded to the average of the eigenfrequency values

Table 5 Presentation of the five biologically inspired design principles implemented in the PETRA IV girder design. The scanning electron microscopic images (© Alfred Wegener Institute, AWI) show a radiolaria (scale bar: 50 μm) (1), and details of the shell structures of

the diatoms *Thalassiosira* sp. (scale bar: 10 μm) (2), *Roperia tessellata* (scale bar: 1 μm) (3), *Thalassiosira punctigera* (scale bar: 2 μm) (4), and *Arachnoidiscus* sp. (scale bar: 10 μm) (5)

Description	Image
(1) <i>Hierarchical structures</i> : Structural elements are arranged according to certain characteristics. In the displayed radiolaria, for example, the hierarchical branching of struts allows a smooth load distribution and a high stiffness. A similar hierarchical structure was implemented in the lower part of the girder structure replacing the cross-struts and the small surface in between that were obtained from the topology optimisation	
(2) <i>Voronoi combs</i> : A Voronoi tessellation implies a subdivision of an area or a space in a certain number of Voronoi cells. These irregular combs are present in many diatom shells, e.g., <i>Thalassiosira</i> sp., leading to high surface stiffening, high eigenfrequencies, and increased energy absorption. In the developed girder, Voronoi combs replaced the initially regular rectangular ribs of four surfaces	
(3) <i>45° oriented ribs</i> : Ribs increase the stiffness of structures, especially in lightweight design components. An orientation of ribs in angles of 45°, which is present in many diatom shells, e.g., <i>Roperia tessellata</i> , raise the torsional stiffness. As the lower order mode shapes of the girder were likely to be characterised by a global girder torsion, these ribs were implemented in the girder structure to increase the eigenfrequencies.	
(4) <i>Round / oval holes</i> : Hollow structures can reduce the mass at the same performance. Round/oval shapes of holes additionally reduce peak stresses. Such hole shapes are present in numerous diatom shell structures, e.g., in <i>Thalassiosira punctigera</i> . Round holes were implemented in the back surface of the girder structure. Besides the weight reduction, the holes are also essential for the subsequent casting process, because they allow the removal of material inside	
(5) <i>Smooth connections</i> : The implementation of smooth connections and transitions between different elements of a structure avoids high local stress. In almost all diatom shells, structural elements are smoothly joined to form the delicate structures. Smooth connections were also adopted to the girder structure. Besides the reduction of peak stresses, it is also necessary for a successful casting process	

detected by the eight accelerometers. Deviations between the simulation results and the measured eigenfrequencies were calculated using the following equation:

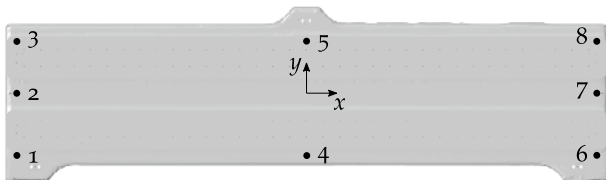
$$\Delta f = \frac{f_{n,\text{exp}} - f_{n,\text{sim}}}{f_{n,\text{sim}}} \cdot 100\%; \quad n = 1, 2, 3, \dots \quad (1)$$

where Δf denotes the frequency deviation, and $f_{n,\text{sim}}$ and $f_{n,\text{exp}}$ are the n th eigenfrequency obtained by simulation and experiment, respectively.

As the impact testing did not involve a force measuring modal hammer, a custom-made MATLAB (The MathWorks, Inc.) script was used to obtain the measured mode shapes (i.e., the displacement of the upper girder surface) from the acceleration data. The first step of the procedure included in the MATLAB script was the double integration of the measured data using the Newton–Cotes formulas (quadrature). Then, the eigenfrequencies were separated applying a 6th order Infinite Impulse Response (IIR) band-pass filter. IIR filters produce filters with sharp frequency cutoff characteristics and only require a small number of

Table 6 Number of volume mesh nodes and elements of the final magnet–girder assembly for the 3 m PETRA IV girder

	Number of nodes	Number of elements
Girder	499,552	2,815,203
Magnets	197,111	920,933
Mashine shoes	1,164	4,202
Bases	35,472	162,810
<i>Total</i>	733,299	3,903,148


Fig. 5 Top view of the bio-inspired girder, in which the positions 1 to 8 of the eight accelerometers are shown in black circles. The considered coordinate system differs from that used in the simulations

coefficients and thus comparably little memory capacity. They are often applied to obtain the amplitude response [58].

After applying a frequency bandpass filter with the range $90\%f_n$ to $110\%f_n$ (f_n denotes the n th eigenfrequency) to the data, the resulting displacement was plotted for each accelerometer in a 3D plot matching the actual accelerometer positions. A movie was created for each mode shape visualising the vibration of the upper girder surface, which was compared to the numerically obtained mode shapes.

3 Results

This sub-chapter presents the results of the girder development process aiming at a biologically inspired PETRA IV girder design.

3.1 Topology Optimisation

The topology optimisation resulted in a continuous structure involving all elements of an artificial element density larger than 0.55 (Fig. 6). At a first glance, the structure reminded of a bridge. It consisted of two large arch-like structures connected to the upper girder surface, which were also interconnected at several positions. The rear arch-like structure was filled with material. At both ends of the front arch-like structure, material was accumulated forming surface-like structures. The convergence plots (see appendix 1) indicated a successful maximisation of the defined optimisation

objective considering the constraints on the maximum static displacement and the volume.

3.2 Abstraction and Cross-sectional Optimisation

The topology optimisation result was abstracted to a beam–shell model to perform a cross-sectional optimisation. As illustrated in Fig. 6, thin, beam-like structures were abstracted as curves/lines, whereas large, surface-like structures were considered as surfaces. The rear, thick arch-like structure was transformed into a biologically inspired sandwich structure with two outer surfaces and inner ribs oriented with an angle of 45° towards the horizontal. The two surfaces on the right and on the left side of the structure were stiffened by applying cellular structures as ribs. In a first step, regular rectangular ribs were applied.

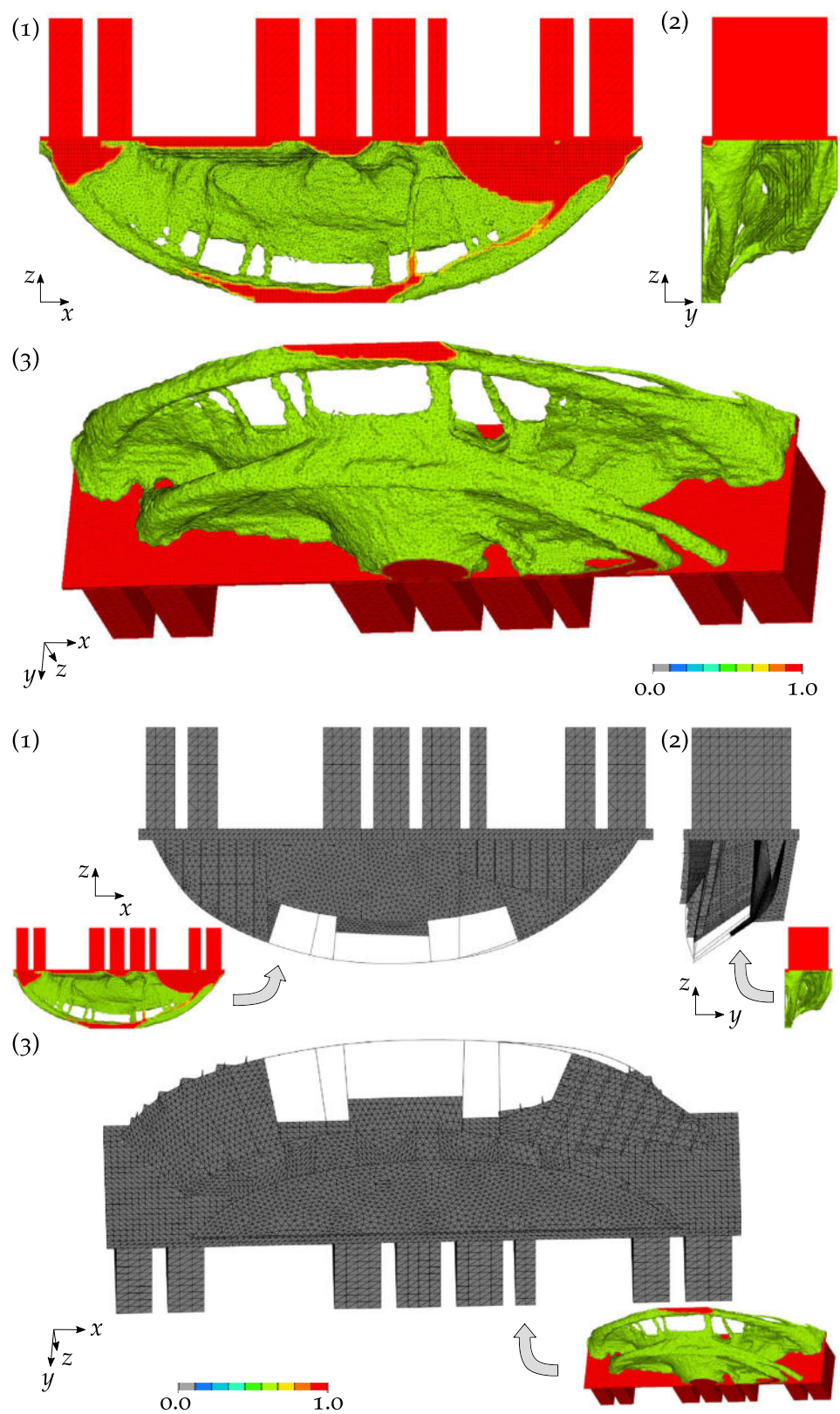
The evolutionary strategic optimisation led to numerous girder structures varying in their parameter values. Figure 7 shows the highest 1st eigenfrequency reached in each generation and the corresponding maximum static displacement and girder mass of that girder structure. All three objectives converged towards a maximised (1st eigenfrequency) or minimised (maximum static deformation and girder mass) value. However, the differences between the objective values of the first and the last generation were only 1.3% (1st eigenfrequency), -3.0% (maximum static deformation), and -2.9% (girder mass) considering equation 1.

Comparing all structures of the first and the last generation (Fig. 8), a general improvement of the whole population can be seen. The structures were pushed towards a higher 1st eigenfrequency, a lower girder mass, and a lower maximum static displacement as it has been defined in the optimisation objectives. Four different parameter combinations were exemplarily highlighted. The structures 1 and 2 showed a very similar maximum static deformation, whereas their girder mass and 1st eigenfrequency varied strongly. In contrast to that, the structures 1 and 4 had a similar girder mass, but differed in their maximum static displacement and their 1st eigenfrequency. In addition, interesting is the comparison of the structures 2 and 3, which were characterised by the same 1st eigenfrequency and also a similar girder mass, but showed very different maximum static displacements.

The girder structure with the highest 1st eigenfrequency (highlighted with a square in Fig. 8) showed a 1st eigenfrequency of 71.8 Hz, a maximum static deformation of 0.047 mm, and a girder mass of 1.84 t. The beam cross-sectional diameters and shell thicknesses leading to this structure are illustrated in Fig. 9. The beam cross-sectional diameters varied from 39.6 mm to 68.8 mm and the shell thicknesses from 13.1 mm to 29.5 mm.

Table 7 summarises the properties of the chosen girder structure with the highest 1st eigenfrequency based on a

Fig. 6 Front view (1), side view (2), and 3D view (3) of the topology optimisation result for the loaded girder structure (*top*) and the abstracted beam–shell model (*bottom*). The topology optimisation result comprises all elements with an artificial element density larger than 0.55 represented by the colouring



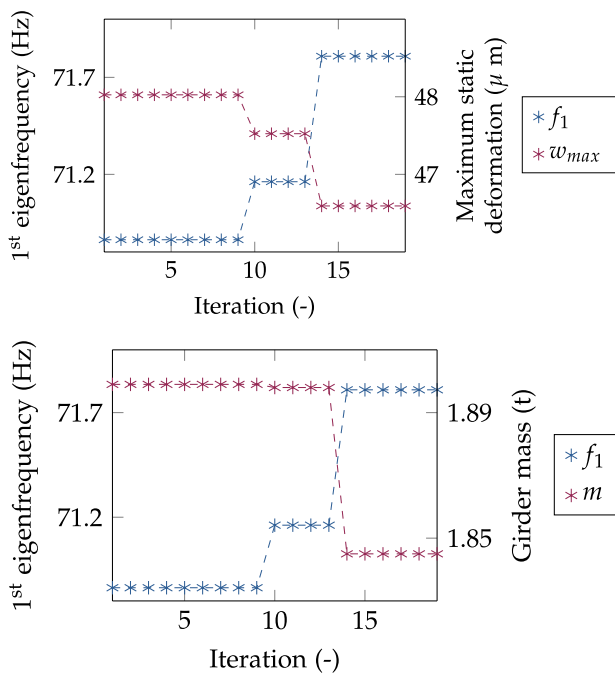


Fig. 7 Cross-sectional optimisation convergence plots for the beam-shell girder model are displayed. For each iteration (generation), the highest 1st eigenfrequency f_1 and the corresponding maximum static deformation w_{max} (top) as well as the corresponding girder mass m (bottom) are given

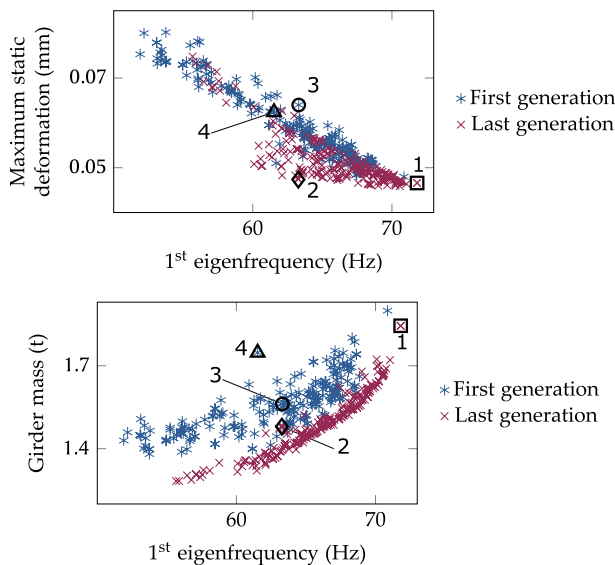


Fig. 8 For all structures of the first and the last generation obtained by the evolutionary strategic cross-sectional optimisation, the 1st eigenfrequency and the corresponding maximum static deformation (top) as well as the 1st eigenfrequency and the corresponding girder mass (bottom) are displayed. Four structures are exemplarily bordered in shape of a square (structure 1), a diamond (structure 2), a circle (structure 3), and a triangle (structure 4)

beam-shell model and a volume model. The results coincided very well showing deviations of maximum 9.2% for the first four eigenfrequencies, 2.0% for the maximum static deformation, and 0.0% for the girder mass. Figure 10 displays the first four mode shapes considering the volume model, which coincided with those of the beam-shell model. All mode shapes showed global girder deformations. In addition, the first two mode shapes were characterised by a strong deformation of the large lower strut.

3.3 Biologically Inspired Structures and Further Structural Adaptation

The final bio-inspired girder design is pictured in Fig. 11 including an illustration of the biologically inspired features implemented in the design. Moreover, the additional structural adaptations due to late changes in the specifications are marked. They include (1) the slight removal of material at the front-left side and at the rear middle creating space for the bases that were moved horizontally towards the beam axis, (2) the small material removal at the lower side of the upper thick surface to make space for the middle screw, and (3) the implementation of material in form of 'ears' at the three support point positions allowing a connection to the machine shoes.

The designed girder made of grey cast iron had a volume of 2.76 m³ and a mass of 2.01 t. The eigenfrequencies of the free, unloaded girder and of the magnet-girder assembly, considering the bases provided by DESY and the machine shoes abstracted as cylinders, are listed in Table 8. The 1st eigenfrequency dropped by 54% comparing the magnet-girder assembly to the free girder.

Figure 12 shows the first four mode shapes of the free, unloaded girder. The 1st eigenmode is a twist around the centre of the upper girder surface. This corresponds to the 1st mode shape of the magnet-girder assembly (Fig. 13). The remaining displayed mode shapes of the magnet-girder assembly differed from those of the free unloaded girder. Nevertheless, they were similar to those of the first volume model (Fig. 10). However, the 1st mode shape showed already a deformation of the bases, which has not been observed for the previously used box-shaped bases.

Regarding the maximum deformation due to gravity of the magnet-girder assembly, the highest value of 53 μm occurred in the middle front of the girder far away from the support points (Fig. 14).

Fig. 9 Structure with the highest 1st eigenfrequency among all structures of the last optimisation iteration was based on the displayed shell thicknesses (circled values) and beam cross-sectional diameters (framed values). The border colours of the dimensions given in mm match the colours of the corresponding shell or beam. The upper girder surface is hidden

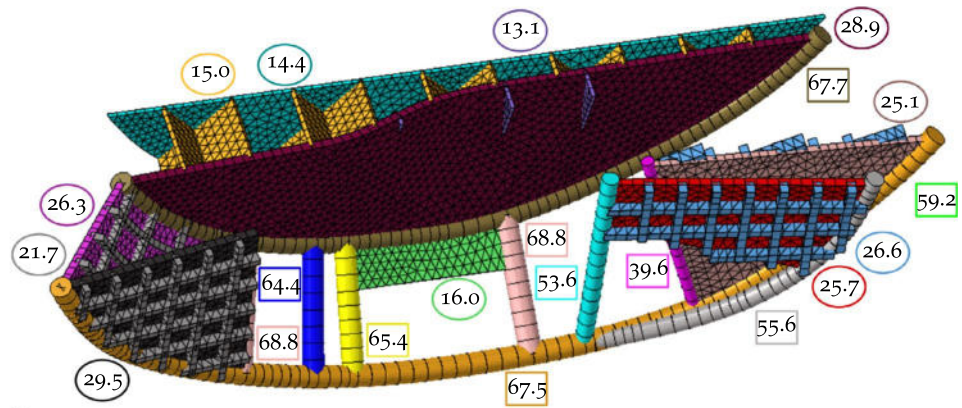
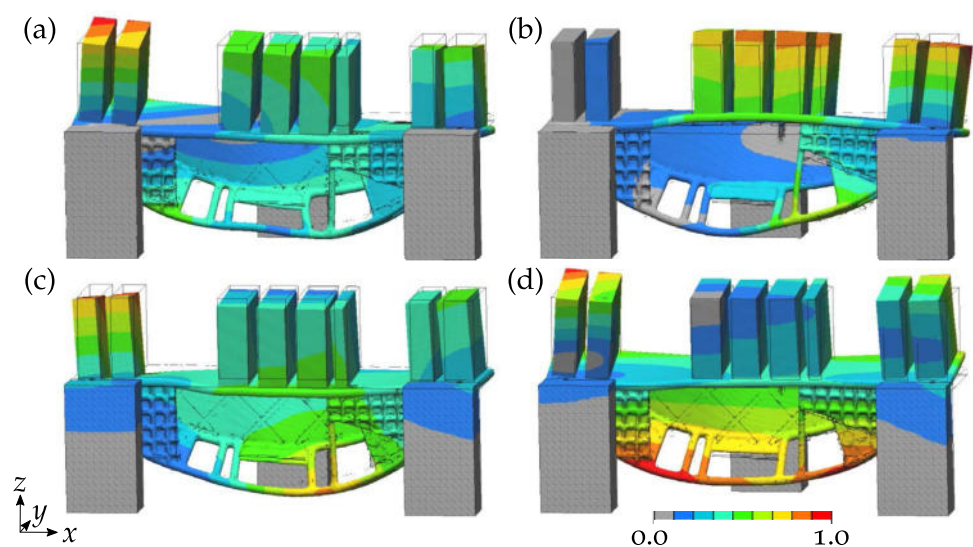


Table 7 First four eigenfrequencies, maximum static deformation due to gravity, and the girder mass for the beam–shell model and the volume model. The deviation of the beam–shell model compared to the

volume model is given. In all models, structural steel S235 was considered as material of the girder and the bases

		Beam/shell model	Volume model	Deviation
Eigenfrequencies	f_1	67.3 Hz	69.3 Hz	-2.9%
	f_2	73.2 Hz	72.8 Hz	0.5%
	f_3	87.4 Hz	96.3 Hz	-9.2%
	f_4	95.1 Hz	104.3 Hz	-8.8%
Maximum static deformation		0.051 mm	0.050 mm	2.0%
Girder mass		1.84 t	1.84 t	0.0%

Fig. 10 1st (a), 2nd (b), 3rd (c), and 4th (d) mode shape of the volume model that resulted from the cross-sectional optimisation. The colours represent the normalised vibration amplitude and the undeformed magnet–girder assemblies are sketched with grey lines. Structural steel S235 is specified as material of the girder and the bases



3.4 Manufacturing and Impact Testing

The designed girder structure was manufactured using the casting technology. Figure 15 shows the manufactured biologically inspired girder.

The impact testing allowed the detection of the first five eigenfrequencies of the free and unloaded bio-inspired

girder, which were visible as peaks in the PSD plot (Fig. 16) that additionally shows the numerically obtained eigenfrequencies. The measured peak at the 2nd eigenfrequency value was not as sharp as the peaks for the other four eigenfrequencies. Moreover, there were several smaller peaks at frequency values below 80 Hz. Likewise, the PSD plot of the floor and the pedestal (Fig. 17) showed

Fig. 11 Rear view (a) and front view (b) of the biologically inspired girder design. The following scanning electron microscopic images (© Alfred Wegener Institute, AWI) of the biological role models are displayed: details of the shell structures of the diatoms *Roperia tessellata* (scale bar: 1 μm) (i), *Thalassiosira* sp. (scale bar: 10 μm) (ii), *Thalassiosira punctigera* (scale bar: 2 μm) (iii), *Arachnoidiscus* sp. (scale bar: 10 μm) (iv), and a radiolaria (scale bar: 50 μm) (v). The additional structural modifications are bordered with dashed black lines and include material removal due to position changes of the bases (1) and due to the location of a large middle screw (2) as well as the implementation of 'ears' (3)

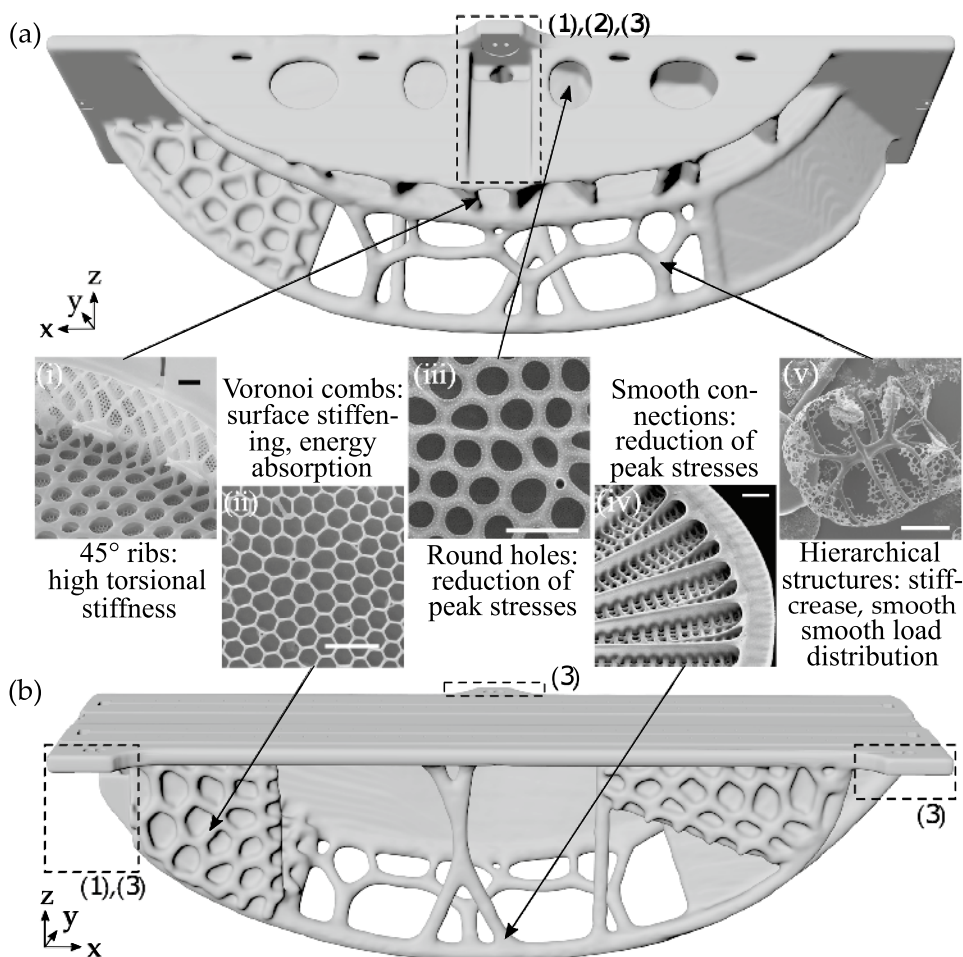


Table 8 First five eigenfrequencies of the free unloaded bio-inspired girder and the magnet-girder assembly considering the bio-inspired girder. Grey cast iron is specified as girder material

	Free and unloaded girder	Magnet-girder assembly
f_1	119.6 Hz	55.0 Hz
f_2	189.8 Hz	59.8 Hz
f_3	236.8 Hz	74.8 Hz
f_4	257.1 Hz	82.7 Hz
f_5	290.4 Hz	94.6 Hz

various peaks between 20 Hz and 80 Hz. In addition, there was a peak at about 150 Hz in the PSD of the pedestal, which was not present in the floor movement.

In Table 9, the measured eigenfrequencies are compared to the numerically obtained values. As it was already visible in the PSD plots, both eigenfrequency values corresponded very well, showing deviations of maximal 5.2%.

The visualisation of the vibration amplitude of the upper girder surface based on hitting the girder on position 8 is displayed in Fig. 18, exemplarily for the

1st eigenfrequency (see also the movie attached as supplementary information). The data obtained by the eight accelerometers allowed the detection of a torsional 1st mode shape, which corresponds to the mode shape obtained by the modal analysis (cf., Fig. 12a). A comparably high displacement was detected at the position 8, where the girder had been hit for this impact testing.

4 Discussion

In this chapter, the results of the girder development process are discussed.

4.1 Topology Optimisation

The topology optimisation converged successfully and the chosen mesh properties were appropriate, since the establishment of clearly defined load paths was possible.

The resulting unsymmetrical structure was comparable to a typical bridge structure. A girder encounters high loads

Fig. 12 1st (a), 2nd (b), 3rd (c), and 4th (d) mode shape of the free and unloaded final biologically inspired girder. The colours represent the normalised vibration amplitude. Grey cast iron is specified as girder material

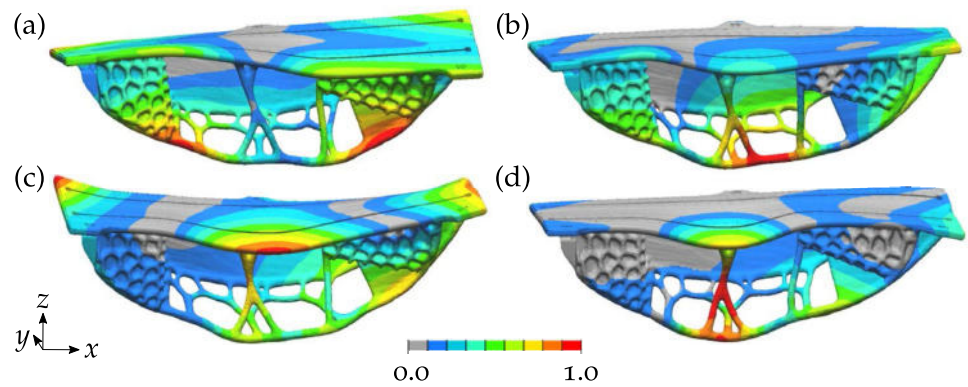


Fig. 13 1st (a), 2nd (b), 3rd (c), and 4th (d) mode shape of the final magnet–girder assembly. The colours represent the normalised vibration amplitude and the undeformed models are sketched with grey lines. Grey cast iron is specified as girder material, spheroidal cast iron as material of the bases

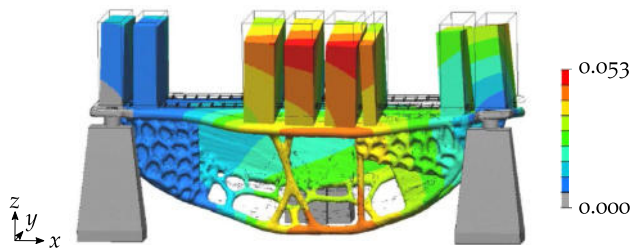
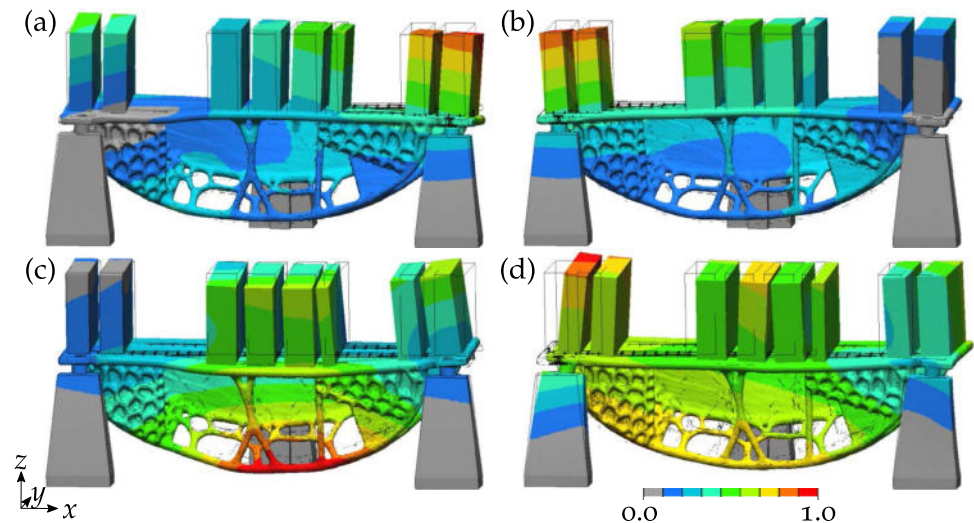


Fig. 14 Deformation due to gravity of the final magnet–girder assembly. The colours represent the deformation in mm and the undeformed model is sketched with grey lines. Grey cast iron is specified as girder material, spheroidal cast iron as material of the bases

due to the heavy magnets it has to carry. Thus, a bridge-like structure was expected to appear, since a maximum static deformation due to gravity was set as a constraint. The non-symmetry of the structure results from the similarly non-symmetrical loading. In addition, it has been stated that topology optimisations with frequency objectives rarely result in symmetrical structures, because the mode shapes

of complex geometries are often non-symmetrical [59]. Regarding compliance minimisation objectives, however, topology optimisations often lead to symmetric structures allowing an equally distributed load path. Consequently, although the here generated structure is non-symmetrical, it still has the appearance of a symmetrical structure that was deformed afterwards.

4.2 Abstraction and Cross-sectional Optimisation

The structure resulting from the topology optimisation was successfully abstracted into a beam–shell model, because both the load paths and the surface-like structures were explicitly visible.

The subsequent cross-sectional optimisation showed a clear convergence of the three optimisation objectives. A comparison of the structures forming the first and the last generation of the optimisation indicated a general improvement of the properties, i.e., the 1st eigenfrequency increased and the maximum static deformation and the mass

Fig. 15 Photos of the manufactured bio-inspired girder in a front view (a) and back view (b). Springs are positioned between the bases and the girder. This setup was used for the impact testing. The photos are printed with permission from Deutsches Elektronen-Synchrotron DESY

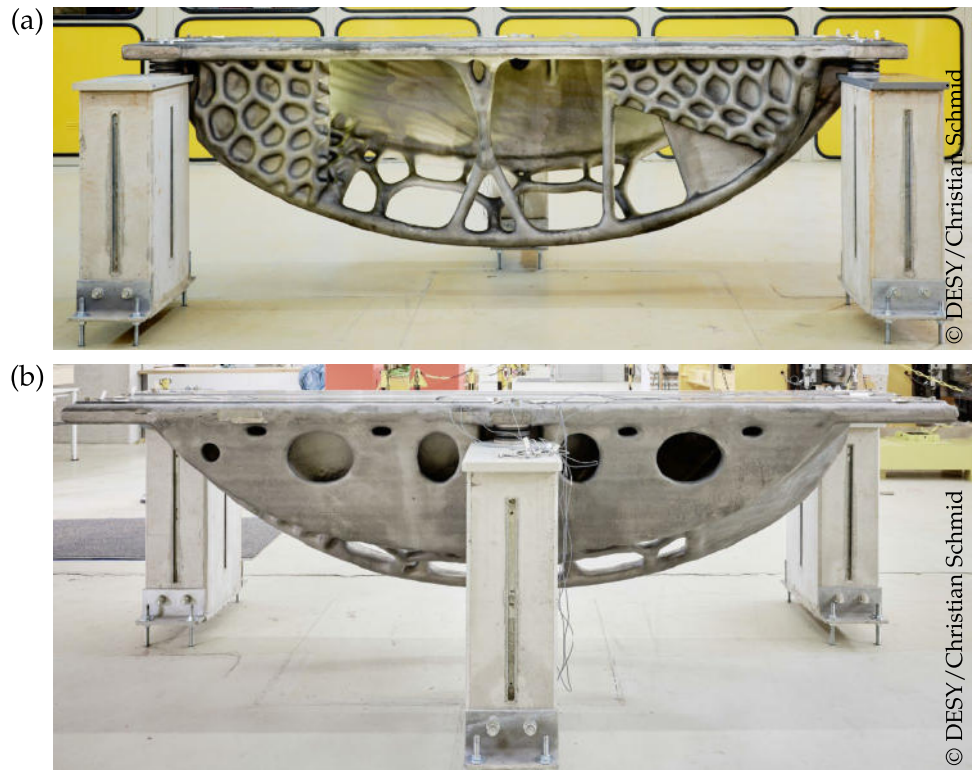
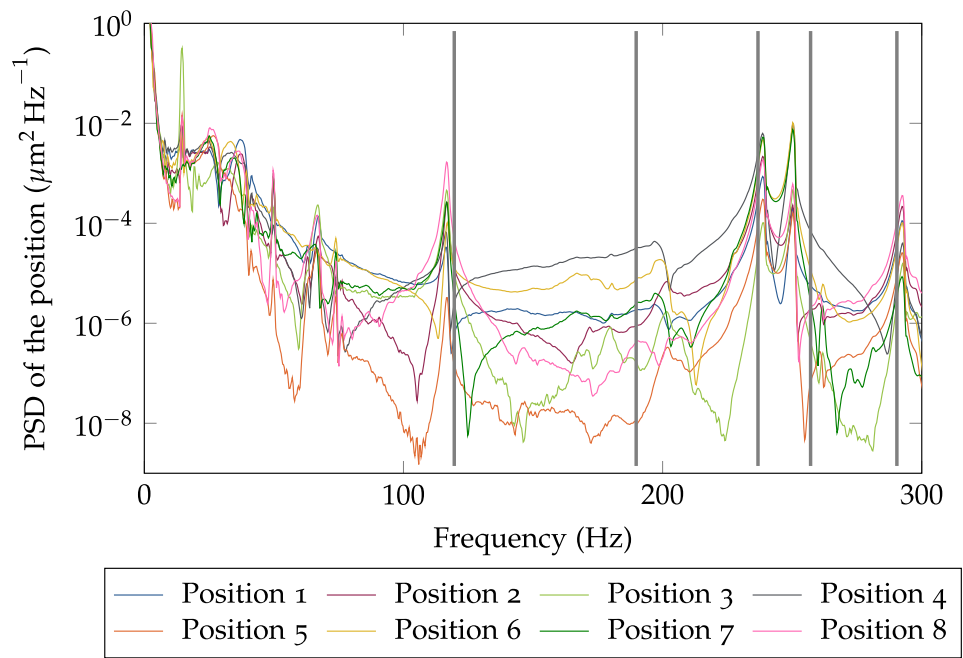


Fig. 16 Power spectral density (logarithmic scale) depending on the frequency obtained by eight accelerometers fixed to the upper surface of the biologically inspired girder. The unloaded girder was positioned on springs and hit with an impact hammer on position 4. The grey vertical lines show the numerically obtained eigenfrequencies



decreased. Thus, it can be concluded that the algorithm worked successfully. However, the cross-sectional optimisation improved the objectives only slightly: the maximum 1st eigenfrequency increase from the first to the last generation was only 1.3%, and the corresponding decrease in the

maximum static deformation and the mass was -3.0% and -2.9% , respectively. The obtained optimum structure was based on cross-sectional values that strongly varied, which possibly shows that the optimisation was yet successful.

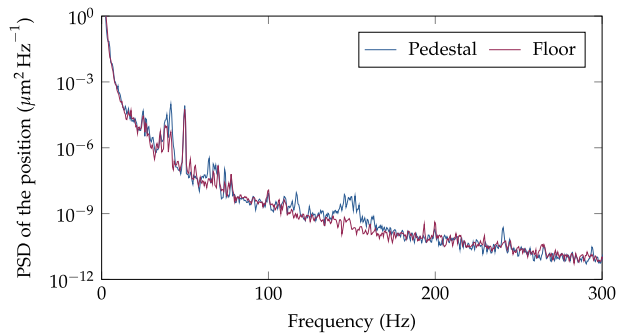


Fig. 17 Power spectral density (logarithmic scale) depending on the frequency obtained by two accelerometers fixed to the floor and to the pedestal, on which is biologically inspired girder was placed

Table 9 First five eigenfrequencies of the free unloaded bio-inspired girder obtained by simulation and by measurements based on impact testing. The measured eigenfrequencies are the mean values of the eight sensors positioned at different locations of the upper girder surface. The deviation between the measured and the simulated eigenfrequencies is also given

	Simulation	Measurement	Deviation
f_1	119.6 Hz	116.6 Hz	-2.5%
f_2	189.8 Hz	199.7 Hz	5.2%
f_3	236.8 Hz	238.7 Hz	0.8%
f_4	257.1 Hz	250.2 Hz	-2.7%
f_5	290.4 Hz	292.5 Hz	0.7%

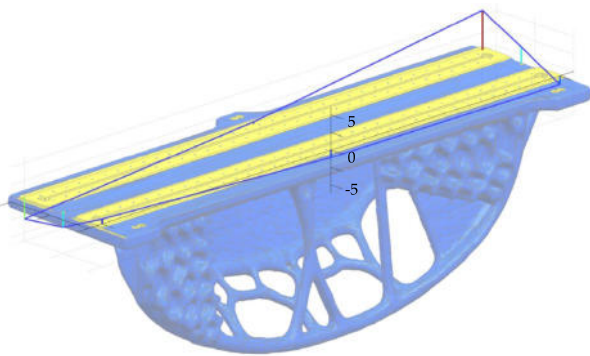


Fig. 18 Visualisation of the measured 1st mode shape of the bio-inspired girder based on eight accelerometers placed on the upper girder surface. The vertical axis shows the displacement in μm

On one hand, the small improvement of the objectives might indicate that the topology optimisation result and the abstraction into a beam–shell model resulted already in a girder structure with very good properties, where the 1st eigenfrequency could almost not be increased further considering the defined boundary conditions. On the other

hand, it is possible that the improvement of the optimisation objectives was limited due to the used optimisation method implemented in the optimiser Octopus. Evolutionary strategic optimisations do not always reveal the best solution, because the algorithm might have followed a local maximum of the fitness landscape instead of the global maximum. Thus, although all defined optimisation objectives converged, they possibly converged towards a local maximum. In addition, the defined optimisation settings and the number of parameters could have influenced the only small improvement of the structures from the first to the last generation.

In general, raising the number of parameters in an evolutionary strategic optimisation certainly increases the computational effort. Thus, although the struts of the girder model were subdivided, the same cross-sectional diameter values were assigned to all subdivisions, because otherwise the number of parameters would have been too large. The large strut in the front of the beam–shell model, for example, certainly plays an important role for the stability of the structure. Varying cross-sectional diameters along the strut could have further improved the girder structure. To study the impact of many parameters on the analysed properties, a combination of the optimisation with a preceding Design of Experiment (DoE) is possible. The DoE identifies the impact of each parameter on the overall objectives. Thus, more parameters (i.e., varying cross-sectional diameters along one strut or different thicknesses applied to one shell) could have been considered. The outcome of the DoE would indicate the parameters strongly influencing the eigenfrequency and the maximum static deformation. Those parameters would have then been included in the subsequent evolutionary strategic optimisation, while less affecting parameters would have been given a constant cross-sectional value. Thus, in continuative studies, the effectiveness of a DoE prior to the evolutionary strategic optimisation should be studied.

The eigenfrequencies and the maximum static deformation due to gravity of the beam–shell model conformed to the corresponding values of the volume model. The appearing deviations of 0.5% to 9.2% (absolute values) can be explained by the different mesh properties and also by small structural adaptations due to transforming the beam–shell model into a volume model. Since neither the structure, nor the mode shape were symmetrical, the small structural adaptations affected some mode shapes (and thus the corresponding eigenfrequencies) more strongly than others. While the 1st and 2nd eigenfrequency coincided by more than 97%, the 3rd and 4th eigenfrequency varied up to 9.2%. The 3rd and 4th mode shapes involved not only a girder deflection, but also deformations of the bases, which did not occur for the 1st and 2nd mode shape. A detailed view on the connection between girder and bases shows that the transformation of the beam–shell model into the volume

model made the corners of the upper girder surface round (Fig. 19). This involved the removal of material at the connection point to the beam that connected the girder and the bases. Thus, more RBE3 were necessary to connect the beam to the girder, which presumably increased the connection stiffness and thus the eigenfrequencies of the volume model compared to the beam–shell model. However, both models can be seen as plausible, because the mode shapes coincided and the eigenfrequency deviations were small taking the size and the complexity of the structure into account.

4.3 Biologically Inspired Structures and Further Structural Adaptation

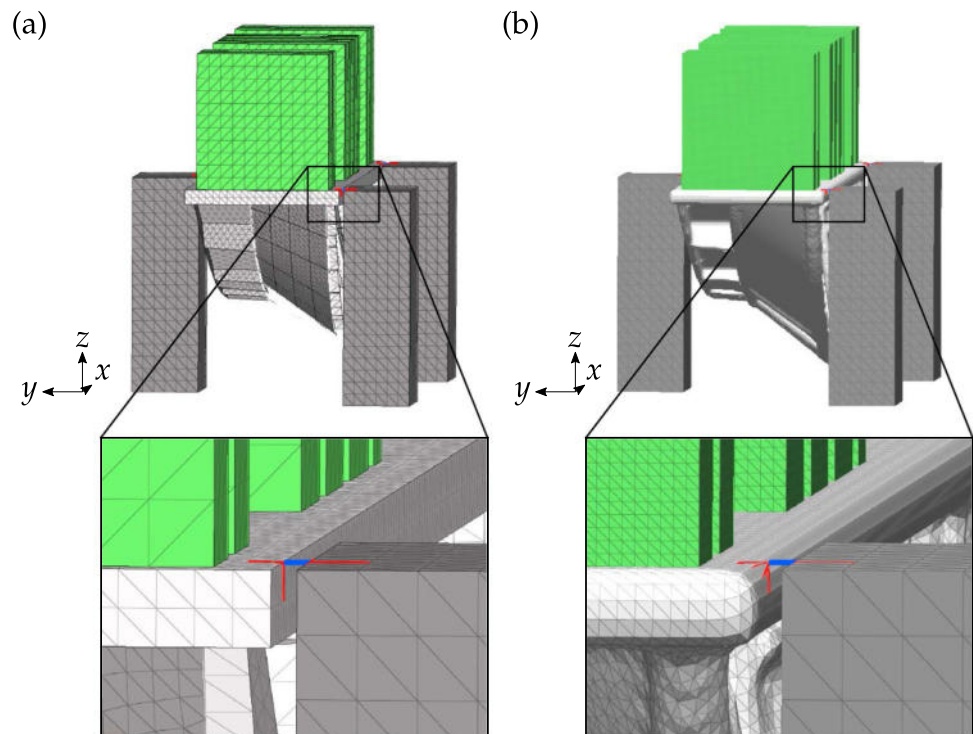
The successful implementation of biologically inspired structures into the girder design led to a complex girder structure with an attractive design.

The comparison of the 1st eigenfrequency of the free and unloaded bio-inspired girder to the 1st eigenfrequency of the free and unloaded PETRA III girder (equipped girder shown in Fig. 1) reveals the same 1st eigenfrequency value (120 Hz vs. 119 Hz) specifying grey cast iron as girder material. Note though, that the PETRA III girder was 4.2 m long, while the length of the here developed girder was 2.9 m. In addition, the definition of the girder support for the bio-inspired girder differs from that for the PETRA III girder. Yet, this comparison is only partly meaningful for the application in the synchrotron facility, because the properties of the loaded

girder positioned on the bases inside the tunnel are relevant and do certainly vary from the properties of the free and unloaded girder.

Comparing the 1st eigenfrequency of the bio-inspired magnet–girder assembly of 55 Hz to the 1st eigenfrequency of 69 Hz of the magnet–girder assembly obtained after the cross-sectional optimisation (volume model) gives a 21% lower 1st eigenfrequency value of the first model. It has to be noted, though, that a comparison of both models is hardly possible, because—aside from the different mesh properties—they varied in the geometry and the material properties of the girder (steel S235 vs. grey cast iron) and the bases (steel S235 vs. spheroidal cast iron). The published parametric study on the impact of the material properties on the magnet–girder assembly had already shown that grey cast iron reduces the 1st eigenfrequency by almost 20% compared to S235 [50]. In addition, the mounting stiffness of the girder has a strong impact on the eigenfrequencies, which has also been investigated in the mentioned parametric study [50]. The mounting stiffness of the final bio-inspired magnet–girder assembly was reduced due to the smaller bases, which is presumably why the 1st mode shape at 55 Hz showed already deformations of the bases. Regarding the initial, cross-sectional optimisation-based magnet–girder assembly, the first deformations of the bases were obtained for the 3rd mode shape at 75 Hz. In addition, previous studies have pointed out that the stiffness of the bases strongly influences the magnet–girder assembly [60]. Thus, future

Fig. 19 Beam–shell model with displayed cross sections (a) and volume model (b) of the best magnet–girder assembly that resulted from the cross-sectional optimisation. For both models, a detailed view on a beam connecting the girder to the bases is given. The models are composed of the girder (light grey), the bases (dark grey), the magnets (green), the beams connecting the girder to the bases (blue), and the RBE3 elements (red)



studies should include an optimisation of the bases' geometry to maximise the stiffness.

While measurements have revealed a 1st eigenfrequency of the magnet–girder assembly used in the PETRA III synchrotron facility of about 35 Hz [53], the numerically obtained 1st eigenfrequency of the here studied magnet–girder assembly was with 55 Hz considerably higher. However, the latter value has to be dealt with caution, because the abstraction of the machine shoes as cylinders might have led to a girder support stiffness varying from the actual one. Therefore, in addition to the vibration measurements of the unloaded and free bio-inspired girder, the eigenfrequencies of the here studied magnet–girder assembly should also be measured to verify the numerical results.

In regard to the impact of the loading on the girder, eigenfrequency measurements of the loaded and the unloaded SOLEIL girder have been conducted [61]. The 1st eigenfrequency of the unloaded girder of 108 Hz dropped by 59% to 44 Hz with added magnets. Assuming that this value can be applied to the here developed PETRA IV girder, the 1st eigenfrequency of 120 Hz of the unloaded girder would decrease to 49 Hz, which is slightly lower than the 55 Hz that were numerically obtained for the magnet–girder assembly. In addition, at APS-U, a 1st eigenfrequency decrease of 10% considering the floor compliance in the numerical model has been stated [55]. Applying this value to the estimated 49 Hz for the 1st eigenfrequency would decrease the 1st eigenfrequency to 44 Hz. However, this 1st eigenfrequency value of the bio-inspired magnet–girder assembly is only hypothetical and based on two studies applied to different magnet–girder assemblies varying in geometry, loading, boundary conditions, and material properties. In addition, applying the 1st eigenfrequency decrease of 59% [61] and of 10% [55] to the PETRA III girder would result in a 1st eigenfrequency of 44 Hz, which is slightly higher than the actually measured 1st eigenfrequency of 35 Hz. Therefore, the mentioned 1st eigenfrequency estimation has to be treated with caution. Yet, it can be concluded that the numerically obtained 1st eigenfrequency value of the bio-inspired magnet–girder assembly might overestimate the real 1st eigenfrequency, which is why the eigenfrequencies should be determined experimentally.

4.4 Manufacturing and Impact Testing

The today's achievements in the field of casting technologies allowed a successful fabrication of the bio-inspired girder structure. Despite the large dimensions and the complexity of the structure, a mould was manufactured and successfully filled with the liquid metal to built the casted part.

Regarding the financial expense, the manufacturing of the here designed girder structure was certainly more expensive

than in the case of simple box-like girders. However, if the higher structural complexity increases the stability of the magnet–girder assembly, and thus of the particle beam, a higher financial expense might be justifiable. Regarding the casting process including 3D printed sand moulds, the cost per part remains constant independent of the part complexity, while the costs for traditional manufacturing processes would rise strongly with increasing part complexity [62]. Thus, in the case of manufacturing the PETRA IV girders using the casting technology with 3D printed sand moulds, a high structural complexity is possible, which might allow very stable magnet–girder assemblies.

The impact testing completed the girder development process. The high correspondence of the numerically obtained eigenfrequencies with the experimental data does not only show that the numerical models are reliable, but it also indicates a successful manufacturing process. Despite the already mentioned complexity of the designed girder, it was possible to produce a casted part without critical blowholes or a significant discrepancy from the modelled geometry.

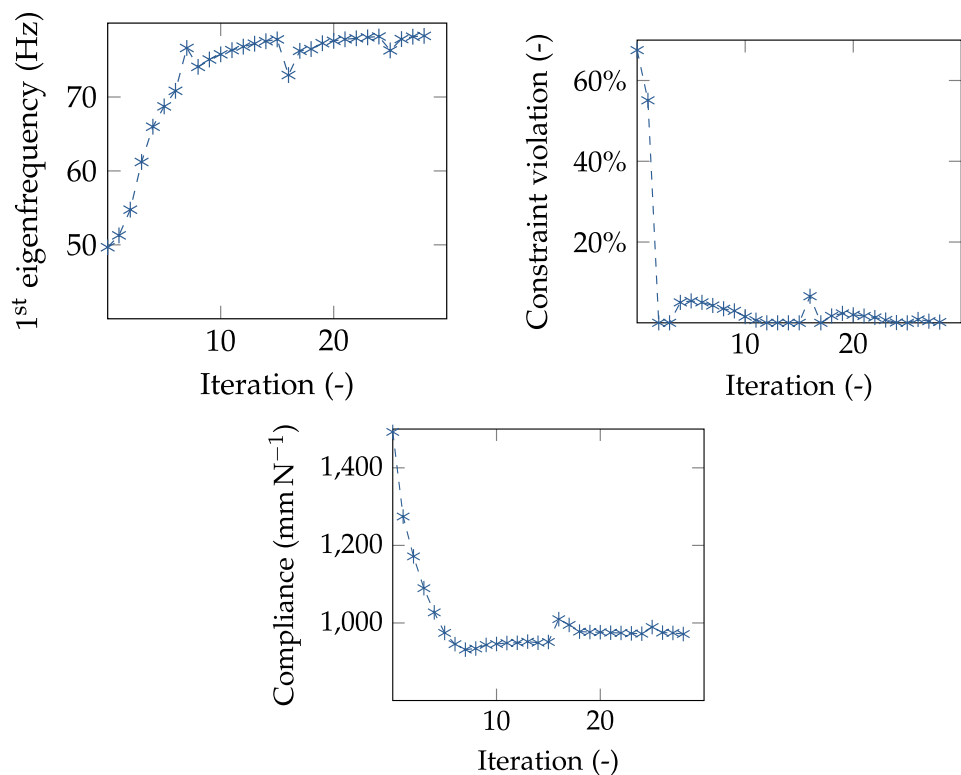
Regarding the obtained PSD of the bio-inspired girder, the less distinct peak at the 2nd eigenfrequency can be explained by the corresponding mode shape, which showed highest vibration amplitudes at the lower part of the girder, whereas the upper girder surface equipped with the accelerometers vibrated less strongly. Nevertheless, the detected 2nd eigenfrequency corresponds to the numerically obtained eigenfrequency by about 95%.

Various peaks appeared at frequencies below 80 Hz. As the peaks were also present in the PSD of the floor and the pedestal, it is concluded that those vibrations result from the in-house noise. In-house noise has also been detected in the ground vibration measurements at DESY [48]. The additional peak at about 150 Hz appearing in the PSD of the pedestals might indicate a resonance frequency of the pedestal. Summing up, the impact testing clearly identified the eigenfrequencies of the unloaded girder, especially when considering the PSD of the floor and the pedestal.

4.5 Outlook

The application of a parametric product development process based on a topology optimisation, the implementation of biologically inspired structures, and an evolutionary strategic cross-sectional optimisation allowed the successful generation of an optimised biologically inspired girder structure for PETRA IV that has been manufactured. The coincidence of the structural eigenfrequencies and mode shapes measured in final experiments to the numerically obtained results validates the conducted methods and the simulation models. However, for the verification of the whole magnet–girder assembly, further experiments are necessary. Especially

Fig. 20 Girder topology optimisation convergence plots of the 1st eigenfrequency (*top left*), the constraint violation (*top right*), and the compliance (*bottom*) depending on the number of iteration



the stiffness of the machine shoes should be determined to include the correct stiffness values into the model. In addition, the stiffness of the ground and the PETRA tunnel should be considered in the model, as studies at different synchrotron radiation facilities noted a strong impact of the ground compliance on the magnet–girder assembly properties (e.g., at the APS-U [55] or at the ESRF–EBS [63]).

In future applications of the here studied girder design process, the process might be complemented by optimising the shape of the implemented bio-inspired structures, e.g., of the Voronoi combs, to further improve the mechanical properties of the girder. In addition, as already mentioned in Sect. 4.2, the beam–shell model obtained from the topology optimisation result should be based on a higher number of parameters allowing a very precise dimensioning of all structural elements of the designed structure. To deal with the numerous parameters, a DoE could identify the parameters strongly affecting the analysed mechanical properties. Subsequently, the cross-sectional optimisation would disclose the optimum diameters and shell thicknesses for those parameters.

Regarding the specifications defined at the beginning of the girder development process, several inputs changed.

These changes imply, for example, the boundary conditions (size of the girder design space) and the loading (magnet properties and position). In addition, specifications relevant for the girder design, which have not been determined yet, should be specified prior to a reapplication of the design development process. These include the alignment system for the magnets and for the girder, because the connection stiffness strongly influences the properties of the magnet–girder assembly. In addition, the design of the bases and the material properties of both the bases and the girder should be defined before re-conducting the girder optimisation. In regard to the material properties, the implementation of composites inspired by nature might also be possible to improve the magnet–girder’s properties even further. Different biologically inspired strategies have been reviewed by [64]. However, it has still to be evaluated if an implementation within the synchrotron machine is possible. The updated specifications for the PETRA IV girder can then be considered in the generated design development process to obtain an adapted girder geometry.

After generating a new girder design based on the adapted specifications, the girder structure should also be studied regarding the thermal deformation. As the PETRA tunnel temperature will be maintained at a constant value, the thermal

deformation for the girder is likely not to be an issue, which is why a thermal load case should not be included in the girder design process. Nevertheless, the thermal behaviour of the structure should be analysed. In addition, studies on the transportation of the loaded girder into the PETRA tunnel have to be carried out, as the transportation could involve structural deformations and thus a misalignment of the components on the girder and/or the girder.

In summary, the generated girder development process has successfully been applied to a 2.9 m long PETRA IV girder. Changes in the specifications and input data can be implemented into the design process to receive adapted girder structures.

5 Conclusion

A development process for a girder structure installed in a synchrotron radiation facility has been generated. Based on a topology optimisation result, a parametric beam–shell model including biologically inspired structures was built up. The subsequent cross-sectional optimisation using evolutionary strategic optimisation revealed an optimum girder structure, which was successfully manufactured using the casting technology. Eigenfrequency measurements validated the numerical models. Future changes in the specifications can be implemented in the development process to obtain adapted girder structures.

Movie of the measured 1st mode shape of the designed and manufactured bio-inspired girder.

Appendix A Convergence Plots

Figure 20 shows the convergence plots of the performed topology optimisation.

Supplementary Information The online version contains supplementary material available at <https://doi.org/10.1007/s42235-023-00373-7>.

Acknowledgements This study was financially supported by the Innovationsfonds from the Alfred Wegener Institute, Helmholtz Centre for Polar and Marine Research (AWI) and by the Deutsches Elektronen-Synchrotron (DESY), a research centre of the Helmholtz Association. The authors acknowledge the comments and suggestions of reviewers.

Funding Open Access funding enabled and organized by Projekt DEAL.

Data Availability The data generated during this study are available from the corresponding author on reasonable request.

Declarations

Conflict of interest The authors have no competing interests to declare that are relevant to the content of this article.

Open Access This article is licensed under a Creative Commons Attribution 4.0 International License, which permits use, sharing, adaptation, distribution and reproduction in any medium or format, as long as you give appropriate credit to the original author(s) and the source, provide a link to the Creative Commons licence, and indicate if changes were made. The images or other third party material in this article are included in the article's Creative Commons licence, unless indicated otherwise in a credit line to the material. If material is not included in the article's Creative Commons licence and your intended use is not permitted by statutory regulation or exceeds the permitted use, you will need to obtain permission directly from the copyright holder. To view a copy of this licence, visit <http://creativecommons.org/licenses/by/4.0/>.

References

- Ljunggren, F., & Ågren, A. (2002). Development of a new damper to reduce resonant vibrations in lightweight steel joist floors. *Applied Acoustics*, 63(11), 1267–1280.
- Anthony, D., Elliott, S., & Keane, A. (2000). Robustness of optimal design solutions to reduce vibration transmission in a lightweight 2-d structure, part i: Geometric design. *Journal of Sound and Vibration*, 229(3), 505–528.
- Bendsøe, M., & Sigmund, O. (2004). *Topology Optimization. Theory, Methods, and Applications* (2nd ed.). Springer-Verlag.
- Díaz, A., & Kikuchi, N. (1992). Solutions to shape and topology eigenvalue optimization problems using a homogenization method. *International Journal for Numerical Methods in Engineering*, 35(7), 1487–1502.
- Tenek, L., & Hagiwara, I. (1994). Eigenfrequency maximization of plates by optimization of topology using homogenization and mathematical programming. *JSME International Journal Ser C Dynamics Control Robotics Design and Manufacturing*, 37(4), 667–677.
- Pedersen, N. (2000). Maximization of eigenvalues using topology optimization. *Structural and Multidisciplinary Optimization*, 20(1), 2–11.
- Du, J., & Olhoff, N. (2007). Topological design of freely vibrating continuum structures for maximum values of simple and multiple eigenfrequencies and frequency gaps. *Structural and Multidisciplinary Optimization*, 34(2), 91–110.
- Xu, B., Han, Y. S., Zhao, L., & Xie, Y. M. (2018). Topology optimization of continuum structures for natural frequencies considering casting constraints. *Engineering Optimization*, 51(6), 941–960.
- Xie, Y., & Steven, G. (1994). A simple approach to structural frequency optimization. *Computers & Structures*, 53(6), 1487–1491.
- Zhao, C., Steven, G., & Xie, Y. (1996). Evolutionary natural frequency optimization of thin plate bending vibration problems. *Structural and Multidisciplinary Optimization*, 11(3), 244–251.
- Huang, X., Zuo, Z. H., & Xie, Y. M. (2010). Evolutionary topological optimization of vibrating continuum structures for natural frequencies. *Computers & Structures*, 88(5–6), 357–364.
- Zhu, J. H., Zhang, W. H., & Qiu, K. P. (2007). Bi-directional evolutionary topology optimization using element replaceable method. *Computational Mechanics*, 40(1), 97–109.
- Panesar, A., Abdi, M., Hickman, D., & Ashcroft, I. (2018). Strategies for functionally graded lattice structures derived using topology optimisation for additive manufacturing. *Additive Manufacturing*, 19, 81–94.
- Simsek, U., Arslan, T., Kavas, B., Gayir, C., & Sendur, P. (2020). Parametric studies on vibration characteristics of triply periodic minimum surface sandwich lattice structures. *The*

- International Journal of Advanced Manufacturing Technology*, 2, 1–16.
15. Wu, J., Aage, N., Westermann, R., & Sigmund, O. (2017). Infill optimization for additive manufacturing—approaching bone-like porous structures. *IEEE Transactions on Visualization and Computer Graphics*, 24(2), 1127–1140.
 16. Gibson, L., & Ashby, M. (1997). *Cellular Solids: Structure and Properties* (2nd ed.). Cambridge: Cambridge University Press.
 17. Seki, Y., Bodde, S., & Meyers, M. (2010). Toucan and hornbill beaks: a comparative study. *Acta Biomaterialia*, 6(2), 331–343.
 18. Seki, Y., Schneider, M., & Meyers, M. (2005). Structure and mechanical behavior of a toucan beak. *Acta Materialia*, 53(20), 5281–5296.
 19. Gibson, L. (1985). The mechanical behaviour of cancellous bone. *Journal of Biomechanics*, 18(5), 317–328.
 20. Round, F., Crawford, R., & Mann, D. (1990). *Diatoms: Biology and morphology of the genera*. Cambridge University Press.
 21. Friedrichs, L. (2014). Biomechanics of diatom frustules—techniques and ecological implications (phdthesis, University of Bremen). Retrieved 2022-07-28, from <https://epic.awi.de/id/eprint/41548/>
 22. Hamm, C., Merkel, R., Springer, O., Jurkojc, P., Maier, C., Prechtel, K., & Smetacek, V. (2003). Architecture and material properties of diatom shells provide effective mechanical protection. *Nature*, 421(6925), 841–843.
 23. Hamm, C. (2005). The evolution of advanced mechanical defenses and potential technological applications of diatom shells. *Journal of Nanoscience and Nanotechnology*, 5(1), 108–119.
 24. Hamm, C., & Smetacek, V. (2007). Armor: why, when, and how. In P. Falkowski & A. Knoll (Eds.), *Evolution of Primary Producers in the Sea* (pp. 311–332). Academic Press.
 25. Losic, D., Rosengarten, G., Mitchell, J., & Voelcker, N. (2006). Pore architecture of diatom frustules: potential nanostructured membranes for molecular and particle separations. *Journal of Nanoscience and Nanotechnology*, 6(4), 982–989.
 26. Diaz Moreno, M., Ma, K., Schoenung, J., & Dávila, L. (2015). An integrated approach for probing the structure and mechanical properties of diatoms: toward engineered nanotemplates. *Acta Biomaterialia*, 25, 313–324.
 27. Gutiérrez, A., Gordon, R., & Dávila, L. (2017). Deformation modes and structural response of diatom frustules. *Journal of Materials Science and Engineering with Advanced Technology*, 15, 105–134.
 28. Heinrichs, A., Frank, P., Siegel, D., & Frank, M. (2017). Bionische Entwicklung einer additiv gefertigten A-Säulen-Verstärkung. *Lightweight Design*, 10, 74–81.
 29. Maier, M., Siegel, D., Thoben, K.-D., Niebuhr, N., & Hamm, C. (2013). Transfer of natural micro structures to bionic lightweight design proposals. *Journal of Bionic Engineering*, 10(4), 469–478.
 30. Maier, M. (2015). Entwicklung einer systematischen vorgehensweise für bionischen leichtbau (phdthesis, University of Bremen). Retrieved 2022-07-28, from <https://media.suub.uni-bremen.de/handle/elib/910>
 31. Koehl, M., & Strickier, J. (1981). Copepod feeding currents: food capture at low Reynolds number 1. *Limnology and Oceanography*, 26(6), 1062–1073.
 32. Keane, A., & Bright, A. (1996). Passive vibration control via unusual geometries: Experiments on model aerospace structures. *Journal of Sound and Vibration*, 190(4), 713–719.
 33. Banerjee, S., & Bhaskar, A. (2009). The applicability of the effective medium theory to the dynamics of cellular beams. *International Journal of Mechanical Sciences*, 51(8), 598–608.
 34. Lou, J., Ma, L., & Wu, L.-Z. (2012). Free vibration analysis of simply supported sandwich beams with lattice truss core. *Materials Science and Engineering: B*, 177(19), 1712–1716.
 35. Lou, J., Wang, B., Ma, L., & Wu, L. Z. (2013). Free vibration analysis of lattice sandwich beams under several typical boundary conditions. *Acta Mechanica Solida Sinica*, 26(5), 458–467.
 36. Ruzzene, M. (2004). Vibration and sound radiation of sandwich beams with honeycomb truss core. *Journal of Sound and Vibration*, 277(4), 741–763.
 37. Xu, M., & Qiu, Z. (2013). Free vibration analysis and optimization of composite lattice truss core sandwich beams with interval parameters. *Composite Structures*, 106, 85–95.
 38. Banerjee, S., & Bhaskar, A. (2005). Free vibration of cellular structures using continuum modes. *Journal of Sound and Vibration*, 287(1), 77–100.
 39. Dai, X., Shao, X., Ma, C., Yun, H., Yang, F., & Zhang, D. (2017). Experimental and numerical investigation on vibration of sandwich plates with honeycomb cores based on radial basis function. *Experimental Techniques*, 42(1), 79–92.
 40. Wang, X., & Stronge, W. (2001). Micro-polar theory for a periodic force on the edge of elastic honeycomb. *International Journal of Engineering Science*, 39(7), 821–850.
 41. Syam, W., Jianwei, W., Zhao, B., Maskery, I., Elmadih, W., & Leach, R. (2018). Design and analysis of strut-based lattice structures for vibration isolation. *Precision Engineering*, 52, 494–506.
 42. Zhao, J. Q., Zhang, M., Zhu, Y., Li, X., Wang, L. J., & Hu, C. X. (2019). Concurrent optimization of additive manufacturing fabricated lattice structures for natural frequencies. *International Journal of Mechanical Sciences*, 163, 105153.
 43. Andresen, S. (2021). Impact of bio-inspired structural irregularities on plate eigenfrequencies. In E. Sapountzakis, M. Banerjee, P. Biswas, & E. Inan (Eds.), *Proceedings of the 14th international conference on vibration problems. Lecture notes in mechanical engineering* (p. 1117–1125). Springer.
 44. Cheng, L., Liang, X., Belski, E., Wang, X., Sietins, J., Ludwick, S., & To, A. (2018). Natural frequency optimization of variable-density additive manufactured lattice structure: theory and experimental validation. *Journal of Manufacturing Science and Engineering*, 140(10), 105002.
 45. Andresen, S., Bäger, A., & Hamm, C. (2020). Eigenfrequency maximisation by using irregular lattice structures. *Journal of Sound and Vibration*, 465, 115027.
 46. Schroer, C., Agapov, I., Brefeld, W., Brinkmann, R., & Chae, Y.-C. (2018). PETRA IV: the ultralow-emittance source project at DESY. *Journal of Synchrotron Radiation*, 25(5), 1277–1290.
 47. Willmott, P. (2019). *An introduction to synchrotron radiation. techniques and applications* (2nd ed.). John Wiley & Sons Inc.
 48. Schroer, C., Röhlberger, R., Weckert, E., Wanzenberg, R., Agapov, I., Brinkmann, R., Leemans, W. (2019). PETRA IV. upgrade of PETRA III to the ultimate 3d x-ray microscope. conceptual design report (Tech. Rep.). Deutsches Elektronen-Synchrotron DESY, A Research Centre of the Helmholtz Association.
 49. Zhang, L. (2017). Beam stability consideration for low emittance storage ring. (Presentation at the Workshop on Ambient Ground Motion and Vibration Suppression for Low Emittance Storage Rings (GM 2017), Beijing, China)
 50. Andresen, S. (2021). Impact of different components and boundary conditions on the eigenfrequencies of a magnet-girder assembly. *Instruments*, 5, 3.
 51. Sharma, S., Rusthoven, B., Ravindranath, V., Doose, C. (2005). Design of accelerator girder system for vibration suppression. Retrieved 2022-07-28, from (Presentation at the Workshop on Ambient Ground Motion and Civil Engineering for Low Emittance Electron Storage Ring, Hsinchu, Taiwan) <https://www.yumpu.com/s/VjBOR4qhxEFppWCg>
 52. Bialowons, W., Amirikas, R., Bertolini, A., Kruecker, D. (2006). Measurement of ground motion in various sites. C. Biscari, H. Owen, C. Petit-Jean- Genaz, J. Poole, & J. Thomason (Eds.),

- Proceedings of the european particle accelerator conference 2006, edinburgh, uk. Geneva (Switzerland): JACoW Publishing. Retrieved 2021-08-02, from <http://accelconf.web.cern.ch/e06/PAPERS/MOPLS064.PDF>
53. Meyners, N. (2019). *Vibration: PETRA III water on/off*. Presentation at the PETRA IV Tech: Forum, Deutsches Elektronen Synchrotron DESY (unpublished).
 54. Liu, Z., Nudell, J., Preissner, C., Collins, J., & Cease, H. (2016). Optimization for the APS-U magnet support structure. In I. Costa, D. López, M. Prieto, & V. Schaa (Eds.), *Proceedings of the 9th mechanical engineering design of synchrotron radiation equipment and instrumentation conference* (pp. 254–256). Geneva (Switzerland): JACoW Publishing.
 55. Nudell, J., Liu, Z., Preissner, J., Collins, J., & Cease, H. (2016). Preliminary design and analysis of the FODO module support system for the APSU storage ring. In I. Costa, D. López, M. Prieto, & V. Schaa (Eds.), *Proceedings of the 9th mechanical engineering design of synchrotron radiation equipment and instrumentation conference* (pp. 83–86). Geneva (Switzerland): JACoW Publishing.
 56. Laumanns, M., Zitzler, E., Thiele, L. (2001). On the effects of archiving, elitism, and density based selection in evolutionary multi-objective optimization. E. Zitzler, K. Deb, L. Thiele, C. Coello Coello, & D. Corne (Eds.), *Evolutionary multi-criterion optimization. emo 2001. lecture notes in computer science* (p. 181-196). Berlin, Heidelberg (Germany), New York (USA): Springer.
 57. Wang, J., Sama, S., & Manogharan, G. (2018). Re-thinking design methodology for castings: 3d sand-printing and topology optimization. *International Journal of Metalcasting*, 13(1), 2–17.
 58. Oshana, R. (2006). 4 - overview of digital signal processing algorithms. R. Oshana (Ed.), *Dsp software development techniques for embedded and real-time systems* (p. 59-121). Burlington (USA): Newnes.
 59. Warwick, B., Mechefske, C., & Kim, I. (2019). Topology optimization of a pre-stiffened aircraft bulkhead. *Structural and Multi-disciplinary Optimization*, 60(4), 1667–1685.
 60. Andresen, S. (2018). Optimizing the PETRA IV girder by using bio-inspired structures. In V. Schaa, K. Tavakoli, & M. Tilmont (Eds.), *Proceedings of the 10th mechanical engineering design of synchrotron radiation equipment and instrumentation conference* (pp. 297–301). Geneva (Switzerland): JACoW Publishing.
 61. Giorgetta, J.-L. (2004). Measurements on s.r girder prototype. (Presentation at the 8th Machine Advisory Committee MAC meeting (unpublished))
 62. Upadhyay, M., Sivarupan, T., & El Mansori, M. (2017). 3d printing for rapid sand casting - a review. *Journal of Manufacturing Processes*, 29, 211–220.
 63. Cianciosi, F., Zhang, L., Brochard, T., Marion, P., Goirand, L., Dabin, Y., & Lesourd, M. (2016). The girders system for the new esrf storage ring. *Presentation at the 9th Mechanical Engineering Design of Synchrotron Radiation Equipment and Instrumentation Conference (MEDSI)* http://accelconf.web.cern.ch/medsi2016/talks/tuca06_talk.pdf. Retrieved 28 July 2022.
 64. Peng, X. C., Zhang, B. J., Wang, Z., Su, W., Niu, S. C., Han, Z., W., & Ren, L. Q. (2022). Bioinspired strategies for excellent mechanical properties of composites. *Journal of Bionic Engineering*, 19(5), 1203–1228.

Publisher's Note Springer Nature remains neutral with regard to jurisdictional claims in published maps and institutional affiliations.